THE JOURNAL OF PHYSICAL CHEMISTRY C
A JOURNAL OF THE AMERICAN CHEMICAL SOCIETY

pubs.acs.org/JPCC

Article

Effects of Ultraviolet Illumination on Oxygen Interstitial Injection from TiO_2 under Liquid Water

Heonjae Jeong and Edmund G. Seebauer*

Cite This: J. Phys. Chem. C 2022, 126, 20800−20806

Read Online

ACCESS | Metrics & More | Article Recommendations | Supporting Information

ABSTRACT: Super-band-gap illumination influences the reaction rates of semiconducting oxide surfaces with gases and liquids, so it seems plausible that illumination also affects the analogous rates of surfaces with point defects in the interior of the solid. However, such effects have not been investigated. The present paper fills that gap by employing isotopic self-diffusion measurements to demonstrate ultraviolet-enhanced creation of oxygen interstitial atoms from rutile TiO_2(110) surfaces exposed to liquid water. Illumination affects both the injection rate and the mean diffusion length into the solid, although by different mechanisms. These effects offer a new means to enhance post-synthesis defect tailoring via oxide surfaces.

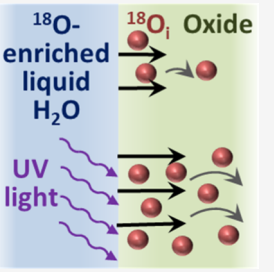

1. INTRODUCTION

Super-band-gap illumination of metal oxide surfaces has long been known to influence rates of adsorption,[1,2] desorption,[2−4] and surface chemical reactions[5,6] with gases and liquids. Numerous possible technological applications have been extensively reviewed.[7−9] TiO_2 enjoys special attention because of favorable material attributes,[10] but other semiconducting oxides such as ZnO,[6] SnO_2,[5,11] and WO_3[12] respond to photostimulation as well. It seems plausible that super-band-gap illumination may affect the reaction rate between oxide surfaces and point defects in the underlying bulk, and useful technological applications may ensue. Indeed, such effects are already known to occur for elemental silicon[13] and for surface diffusion on amorphous TiO_2.[14] A rudimentary understanding of surface-defect chemistry for oxides has emerged only recently,[15−18] and accumulating evidence suggests that it exhibits richness comparable to surface chemistry with gases and liquids.

Surface-defect reactions offer a unique approach to post-synthesis tailoring of concentrations and spatial distributions of defects. A very recent work[17] has shown that poison-free binary oxide surfaces inject oxygen interstitials (O_i) when contacted with liquid water near room temperature. The injection rate is sufficient to eliminate oxygen vacancies in the near-surface bulk, so that O_i becomes the dominant O-related point defect. Such a low temperature accesses a regime wherein equilibrium concentrations of native defects are negligible and kinetic effects dominate defect behavior. New technological possibilities arise, such as complexation reactions with adventitious donors[19] such as hydrogen. Annihilation reactions with oxygen vacancies could also be beneficial as vacancies influence properties such as electrical conductivity,[20] superconductivity,[21] ferromagnetism,[22] carrier lifetimes,[23] and chemical reactivity.[23]

This regime also enables possibilities for rate enhancement through photoexcitation by low-intensity super-band-gap illumination, as the concentration of thermally generated minority carriers is very low. However, such phenomena have not been demonstrated for oxides. The present paper fills that gap by employing isotopic self-diffusion measurements to demonstrate that ultraviolet (UV) illumination increases the rate of O_i injection from rutile TiO_2(110) surfaces exposed to liquid water. The mean diffusion length and effective diffusivity of O_i also increase. Likely mechanisms for these effects are outlined.

2. METHODS

Protocols followed for the isotopic self-diffusion experiments were detailed elsewhere,[17] with the primary change being addition of optical light sources to the apparatus for some experiments. In brief, single-crystal specimens of TiO_2 were immersed in ^{18}O-labeled water (10 atomic % ^{18}O, Sigma-Aldrich) for 60 min at constant temperatures ranging between 30 and 80 °C. The (110) crystallographic orientation was chosen because an extensive literature base already exists, and the nonpolar structure minimizes the likelihood of surface reconstructions under water that would complicate comparisons to first-principles calculations. Rutile TiO_2(110) specimens (MTI Corp) of dimensions 5 × 5 × 0.5 mm were initially prepared by degreasing with successive 10 min ultrasonic baths in acetone, isopropanol, ethanol, and

Received: August 8, 2022
Revised: November 16, 2022
Published: December 1, 2022

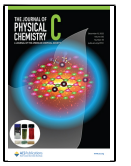

methanol. This was followed by wet etching (1:2 of 30% NH_4OH/H_2O) at room temperature for 40 min in order to remove foreign-element poisons that inhibit O_i injection. Examination of the surfaces by atomic force microscopy showed an rms roughness of 0.23 ± 0.03 nm for the as-received material and 0.14 ± 0.08 nm after wet etching. After isotopic exchange, ^{18}O concentration profiles were measured by ex situ secondary ion mass spectrometry (SIMS) in a time-of-flight mode using a PHI-TRIFT III instrument. A 3 keV Cs ion beam source was employed. For calibration, ^{18}O concentrations were normalized by the known natural abundance ^{18}O concentration (0.2%) measured with the as-received specimens. Profiles were measured at two to five different locations on a given specimen's surface. For some specimens, X-ray photoelectron spectroscopy (XPS) was employed to determine the surface elemental composition and chemical state.

In some experiments, the surfaces were illuminated with either sub-band-gap (red, diode laser) or super-band-gap (UV lamp) light. Red light originated from a diode laser source (CPS635R, Thorlabs) operating at a wavelength of 635 nm and an output power of 1.2 mW. With a roughly Gaussian beam diameter of about 3 mm at the specimen surface, the incident intensity was about 20 mW cm^{-2}. UV light originated from an inspection lamp (Black-Ray B-100AP/R, UVP) operating with a central wavelength of 365 nm. At a distance of 25 cm, the lamp produced an intensity of about 5 mW cm^{-2} at the surface. The intensity was kept low in order to minimize possible heating by light absorption. In the absence of these light sources, some experiments were performed in a darkened room, while others were performed with the fluorescent lighting typical of a laboratory setting. Control experiments showed no significant difference in the diffused profiles between these two conditions.

3. RESULTS

Figure 1 shows representative isotopic ^{18}O profiles for TiO_2 with UV illumination, comparing several temperature conditions. The details of profile shapes sometimes exhibited noticeable variability, especially in the near-surface region within the first 7−10 nm. XPS combined with SIMS performed at several locations on single specimens, as well as among specimens, showed variable adsorption of adventitious impurities including various carbon-containing species. These species not only poison injection sites but also influence buildup of electrical charge on the surface, which influences profile shape dramatically in the space charge layer (SCL) near the surface.[24] Such adventitious adsorption proved difficult to control and often varied across the surface of a single specimen. We therefore focus attention on the deeper-bulk profiles, where such variations exert less influence.

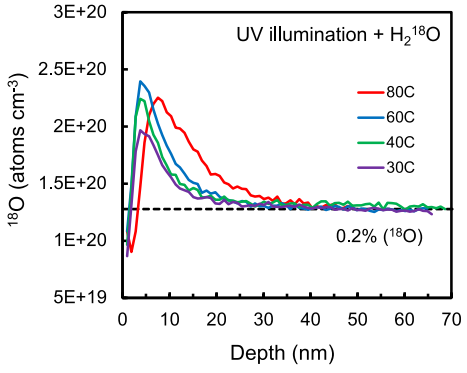

Figure 1. Isotopic ^{18}O concentration profiles for $TiO_2(110)$ immersed in isotope water at several different temperatures for 1 h with UV illumination. The dashed line represents the natural abundance ^{18}O concentration.

Figure 2 shows example profiles comparing profiles with illumination and in the dark at several representative temperatures. Generally, profiles with illumination exhibit higher peak concentrations, deeper penetration, or both compared to those in the dark. To quantify these effects, we computed profile metrics using an analytical mesoscale approach based on the slopes and intercepts of suitably normalized profiles.[25] The approach employs coupled partial differential equations to describe the time evolution of a single mobile form and a stationary form of the isotopic label. It is assumed that diffusion of the label occurs via a mobile intermediate (such as O_i) that sequesters permanently upon encountering trapping sites having a concentration that is spatially and temporally constant. Solution of the differential equations leads to profiles having exponential shapes that are fitted by

$$\ln\left(\frac{C - C_0}{C_0^T - C_0}\right) = \ln\left(\frac{F}{\lambda[C_O^T - C_O]}t\right) - \frac{x}{\lambda} \quad (1)$$

where C denotes the measured concentration of ^{18}O, C_0 denotes the natural abundance concentration of ^{18}O, C_O^T is the total concentration of the lattice sites that exchange with O_i, t represents the diffusion time, and x is the spatial coordinate with $x = 0$ referring to the surface. The slope of the normalized profile yields λ. The intercept yields F, which is assumed to remain temporally constant. Combination of these two parameters yields the effective diffusivity D_{eff} according to

$$D_{eff} = \frac{F\lambda}{[C_0^T - C_0]} \quad (2)$$

F and D_{eff} were adjusted by a factor of 10 to account for the 10% isotopic enrichment of the water.

Figure S1 in the Supporting Information shows example fits of the profiles to eq 1. Linearity is good, suggesting that eq 1 represents a satisfactory functional form. As an independent confirmation of the validity of eq 1 for computing F, the values from this model match within experimental error the values obtained by integrating the areas under the profiles and assuming a constant flux. Even with this confirmation, however, the significance of λ must be evaluated judiciously. There may be multiple mobile species (e.g., different charge states of O_i), multiple kinds of trapping sites, some of which may saturate. In addition to these complications, the Discussion section describes several other mechanisms by which the concentration of trapping sites may vary in space or time. It is not difficult to imagine scenarios where profiles normalized according to eq 1 look approximately exponential within the uncertainty of the profile measurements. Even in such cases, however, λ remains useful as a phenomenological metric.

Figure 3 shows Arrhenius plots for F, λ, and D_{eff}. The data for all three parameters exhibit considerable scatter for reasons detailed in the Discussion section. However, UV illumination moves the regression lines up at the lowest temperatures for each parameter by factors between 1.4 and 1.6 (between 0.15

https://doi.org/10.1021/acs.jpcc.2c05648
J. Phys. Chem. C 2022, 126, 20800−20806

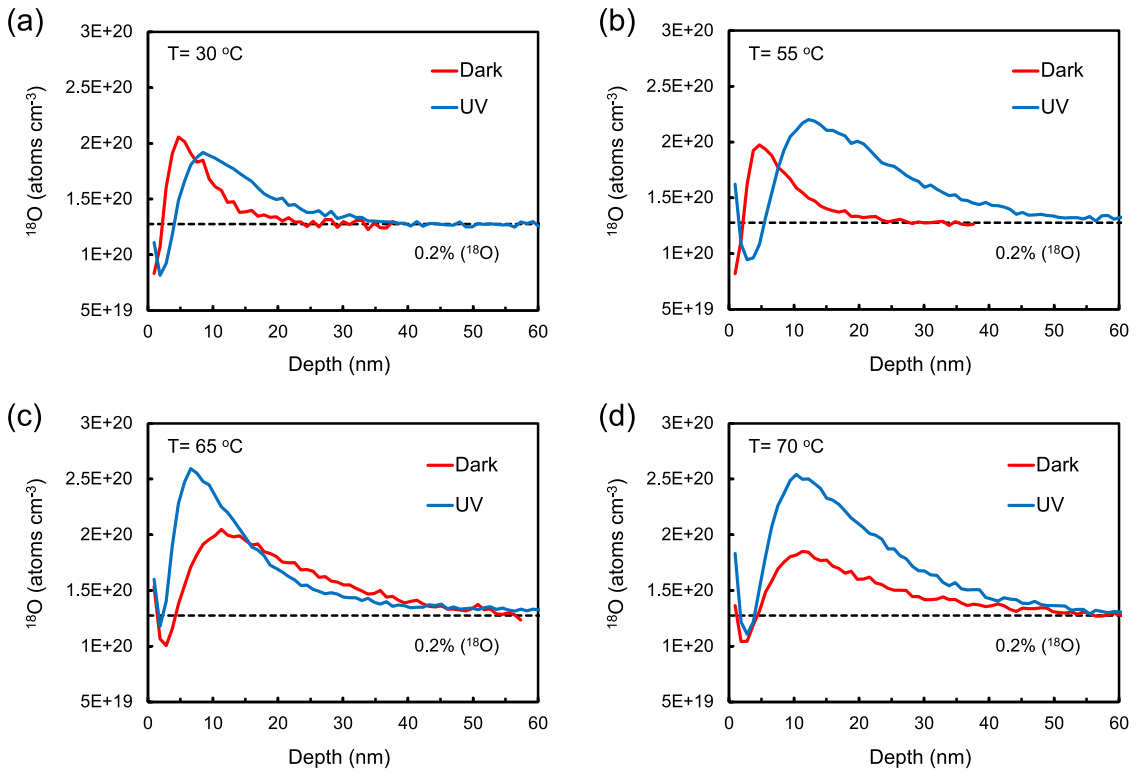

Figure 2. Representative comparisons of isotopic ^{18}O concentration profiles in TiO_2 under dark and UV-illuminated conditions at several diffusion temperatures including (a) 30 °C, (b) 55 °C, (c) 65 °C, and (d) 70 °C. Diffusion time is 1 h.

and 0.2 logarithmic units in Figure 3), thereby making the Arrhenius lines look more horizontal. Tables 1 and 2 respectively, summarize the pre-exponential factors and activation energies for F, λ, and D_{eff}. At first glance, the prefactors and activation energies for all three parameters indicate differences between dark and UV conditions. However, the confidence intervals overlap slightly in all cases, which leaves a marked vulnerability in the case for genuine differences. Indeed, a conventional two-tail Student's t-test to compare the slopes for each parameter yielded probabilities (p-values) for the null hypothesis of 23% for F, 25% for λ, and 21% for D_{eff}. The Supporting Information describes further details of the analysis procedure.

A stronger case comes from comparing the mean values for each parameter—averaged over all temperatures. A conceptually straightforward way to make this comparison employs the regression lines to estimate the value of each data point scaled to the mean temperature (about 58 °C). This scaling procedure quantitatively preserves the standard error characterizing the scatter around the regression lines and enables the use of a t-test to compare the means of the dark and UV data sets. Comparison of the conventional t-statistics computed from the two data sets yielded p-values of 14% for F, 11% for λ, and 12% for D_{eff}. In other words, the likelihood that the difference in means resulted from pure chance is about 1 in 9 to 1 in 7, depending upon the parameter.

4. DISCUSSION

4.1. Treatment of Experimental Uncertainties. The UV intensity was kept low in order to minimize possible heating by light absorption. However, a possible systematic bias in the results could still conceivably result from surface heating. Unequivocal demonstration of nonthermal super-band-gap photostimulation in semiconductors can be challenging as most absorbed light dissipates as heat in the specimen. Increases in a rate parameter could therefore originate from heating, photostimulation, or both.

Perhaps the strongest argument that heating plays a minimal role in the present work stems from the modest temperature dependence of the parameters. Considering D_{eff}, for example, the observed activation energy of about 0.3 eV requires a temperature change of 10 °C to increase the rate by a factor of 1.5—the factor by which the UV regression line differs from the dark in the low-temperature region. An incident intensity of a source power of 5 mW cm^{-2} is unlikely to induce this magnitude of temperature excursion for a surface immersed in water. More importantly, the thermocouple near the surface recorded no observable change in response to switching the source on and off. An increase in specimen temperature by 10 °C should have produced some deflection.

As indicated in the Results section and in an earlier work,[18] the profiles exhibit considerable random variability. XPS combined with SIMS performed at several locations on single specimens, as well as among specimens, showed variable adsorption of adventitious impurities—especially carbon-containing species. Even at sub-monolayer levels,[25] such species can poison injection sites and affect buildup of electrical charge on the surface. The resulting drift forces on charged interstitials can strongly affect profile shape in the adjoining SCL.[24]

Such adventitious adsorption proved difficult to control even across a single specimen. However, profile variability was noticeably smaller for a given specimen than for different specimens. Figure S2 in the Supporting Information shows the data of Figure 3 aggregated specimen-by-specimen. Depending upon the parameter, the confidence intervals for each point

https://doi.org/10.1021/acs.jpcc.2c05648
J. Phys. Chem. C 2022, 126, 20800−20806

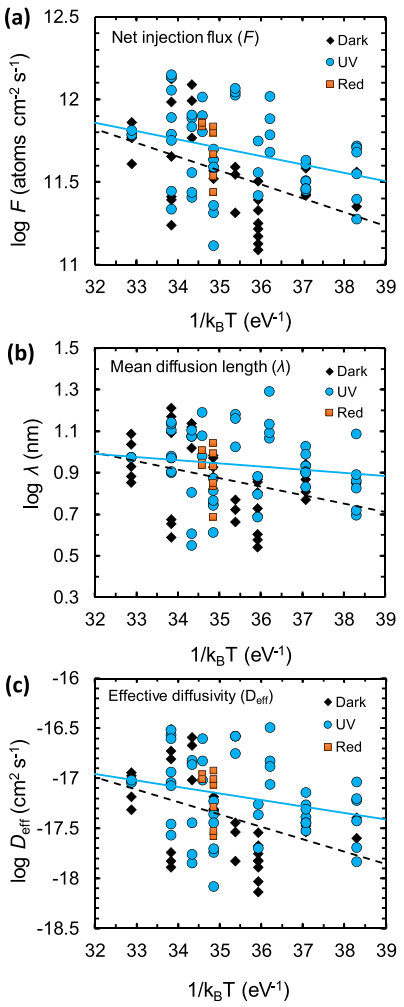

Figure 3. Arrhenius plots for (a) F, (b) λ, (c) D_{eff} for TiO_2(110), comparing conditions in the dark and under UV illumination. Data points are also shown for illumination under red (635 nm) light. The lines represent least squares fits, with red points included as "dark."

Table 1. Effects of UV Illumination on Pre-exponential Factors of Kinetic Parameters for TiO_2

	$\log_{10}$ of pre-exponential factor	
parameter	dark	UV
F (atoms cm^{-2} s^{-1})	14.7 ± 0.8	13.5 ± 0.8
λ (nm)	2.3 ± 0.6	1.5 ± 0.6
D_{eff} (cm^2 s^{-1})	−12.7 ± 1.3	−14.9 ± 1.3

Table 2. Effects of UV Illumination on Activation Energies of Kinetic Parameters for TiO_2

	activation energy (eV)	
parameter	dark	UV
F (atoms cm^{-2} s^{-1})	0.20 ± 0.05	0.12 ± 0.05
λ (nm)	0.10 ± 0.04	0.03 ± 0.04
D_{eff} (cm^2 s^{-1})	0.30 ± 0.09	0.15 ± 0.08

average only 25−50% of the standard error for all points with respect to the corresponding regression line. In other words, reproducibility across a given specimen is significantly better than among different specimens. Despite diligence in using protocols to maintain surface cleanliness, it is likely that adventitious adsorption across a single specimen varies less than among specimens. We therefore believe such adsorption is the single largest contributor to experimental variability. Variable concentrations of extended defects from initial mechanical polishing by the manufacturer may also contribute to profile variations by serving as traps for mobile O. However, all specimens were taken from the same manufacturing lot, which should help to mitigate such effects.

4.2. Effects of Illumination on Injection. Since undoped TiO_2 is n-type and the illumination intensity is modest, UV serves mainly to increase the availability of holes at the surface. As discussed in ref 17, the O-rich conditions of water exposure provide a driving force sufficient for O to enter the solid, thereby leading to its slight oxidation by, for example, filling of O vacancies or complexation with H interstitials. The observed lack in SIMS of H entry into the solid and the requirement of maintaining specimen electroneutrality suggest dissolved H_2 as the most likely reduction product. There is no particular reason this basic picture must change under UV illumination.

F represents the mathematical difference between the rates of elementary-step injection and annihilation and depends upon the concentration of injectable oxygen and the rate constants for injection and annihilation. The fact that only the effective pre-exponential factor changes for F, with the activation energy remaining constant, suggests that the reaction mechanism is largely unchanged by illumination.

On TiO_2, O_i injection from water shares OH deprotonation steps with oxygen evolution reaction (OER),[26,27] as adsorbed oxygen leads to either gaseous O_2 via associative recombination or bulk O_i via injection. It seems likely that O_i injection operates as a side reaction to OER. The reaction network among adsorbed species in OER is complicated,[28] and existing kinetic analyses have not yet included the 2f dumbbell and 3f split configurations of adsorbed O that lead to injection.[15] Photogenerated holes facilitate the deprotonation of OH that lies upstream of O recombination. Such deprotonation also lies upstream of O_i injection,[17] thereby serving to increase F.

F also contains contributions from the reabsorption at the surface of small amounts of O_i that randomly diffuse back to the surface before trapping or disappearing deep into the bulk. In principle, inhibition of this reabsorption could also contribute to an increase in F. The energy barrier for reabsorption generally decreases, however, as TiO_2 becomes less n-type due to greater ease in converting negatively charged O_i in the bulk to neutral forms of O at the surface.[15] Production of extra photoholes under illumination facilitates such conversion and assists in annihilation instead of inhibiting it. Hence, substantial contributions from reabsorption seem unlikely.

The present experiments did not vary the illumination intensity, but it is possible to predict the likely effect under the conditions used here. Oxygen production from water requires four holes for each molecule of O_2, and the quantum yield is highest at low photoexcitation intensities that yield long-lived holes.[29] Electrochemical measurements point to direct charge transfer of these surface holes from the valence band to reactive species with first-order kinetics,[30] and first-principles calculations assume similar kinetics for key elementary steps.[28] At low illumination intensities, characteristic of the present experiments,[29] surface hole concentration should vary linearly in the photocurrent that reaches the surface from the bulk.[31] Photocurrent should in turn scale linearly in illumination

https://doi.org/10.1021/acs.jpcc.2c05648
J. Phys. Chem. C 2022, 126, 20800−20806

intensity.[32−34] It may be inferred that F should also be proportional to illumination intensity.

4.3. Effects of Illumination on Trapping. The parameter λ comprises kinetic quantities from the bulk rather than the surface, so the dependence on UV illumination yields insights different from those associated with F. With a hopping barrier of 0.6−0.7 eV,[35] O_i exhibits significant mobility in TiO_2 even at room temperature. Thus, ^{18}O that is stable in shelf storage and visible in SIMS exists in a sequestered form rather than as freely hopping O_i. That said, irreversible immobilization of O_i in traps having spatially and temporally uniform concentration leads to values of λ from eq 1 that are independent of the hopping diffusivity.[25]

UV illumination may affect λ by multiple mechanisms. One mechanism involves altering the stability of the trapped state of O_i, which translates into a change in the trap concentration. Likely trapping sites for O_i include O vacancies, extended defects, and point defects such as adventitious hydrogen in interstitial form (H_i). These latter defects form complexes with O_i that exist in multiple charge states.[17] Indeed, the association reaction of O_i and H_i yielding the O_i-H_i complex as a product represents a form of Bronsted acidbase chemistry in the solid state. The most stable charge state of O_i−H_i changes in the presence of sizable concentrations of photoholes. Analogous phenomena involving charged defects occur in Si.[36] The photo-induced changes in relative populations of the various charge states affects the total amount of O_i that can be trapped, which translates into variations in λ.

A second mechanism exists for UV illumination to affect λ that involves band flattening in the SCL near the surface, which influences the concentration of trap complexes in that layer. Acid-base reactions between the TiO_2 surface and water lead to build-up of a net charge on the surface at values of pH differing from the isoelectric point (which is equivalent to the point of zero charge if no specific adsorption occurs[37]). For rutile TiO_2, this point varies with incorporated impurities[38] and roughness,[39] but averages to a pH of about 5,[40−43] with a standard deviation of 0.8.[43] Thus, excess negative charge exists on the surface under the pH 7 conditions employed here. This charge leads to the formation of a depletion-type SCL near the surface, assuming that the rutile is n-type. UV illumination of sufficient intensity flattens the bands near a semiconductor surface by exciting minority carriers that drift to the surface and neutralize the excess charge there. Depending upon the ionization levels of the O_i complex and the degree of band flattening, the dominant charge state of the complex may change within the SCL, leading to spatial variations in trapping efficiency that will change the effective value of λ.

4.4. Effects of Illumination on Diffusivity. The parameter D_{eff} represents the effective diffusivity. Under the assumptions leading to eq 1, D_{eff} depends entirely upon F and λ, and neither of these latter parameters depends upon the hopping diffusivity. However, if F varies with time (perhaps due to increasing reabsorption of O_i at the surface as the profile evolves) or if λ varies with either space or time as discussed above, D_{eff} is likely to have contributions from (among other things) the hopping diffusivities and concentrations of various mobile species.

In dark, n-type rutile TiO_2, under the conditions of the present experiments, the principal diffusing species is the O_i^{2-} split configuration[35] with a hopping barrier of 0.65 eV from first-principles calculations.[15] In a p-type material, however, the neutral O_i^0 dumbbell configuration dominates with a corresponding hopping barrier of 0.59 eV.[35] In the presence of illumination that generates photoholes, the concentration of neutral O_i increases, leading to an increase in the contribution of O_i^0 to the diffusional flux and a corresponding decrease in the amalgamated activation energy. Quantitative modeling would require a full-blown kinetic model akin to that developed elsewhere for Si,[36] but even this qualitative treatment suggests that it is plausible for D_{eff} to increase under illumination.

5. CONCLUSIONS

This work demonstrates that low-level super-band-gap illumination of rutile TiO_2 increases the injection flux and mean diffusion length. UV probably affects the injection flux by increasing the rate of OH deprotonation in a manner akin to OER. UV probably affects the diffusion length through the concentration of charged complexes between O_i and adventitious extrinsic defects such as H. UV may influence the stability of a key charge state directly through capturing photoholes or indirectly by flattening the bands in the SCL. Super-band-gap stimulation offers a way to enhance surface-based tailoring of point defect concentrations and spatial distributions during processing steps implemented after initial oxide synthesis. UV illumination may be used in combination with other approaches[17] that are likely to accelerate complete OH deprotonation, such as variation of pH and application of electrochemical potentials. We speculate that combining these approaches will lead to phenomena of comparable complexity to that observed in photoelectrochemistry.

■ ASSOCIATED CONTENT

Supporting Information

The Supporting Information is available free of charge at https://pubs.acs.org/doi/10.1021/acs.jpcc.2c05648.

Representative normalized isotopic ^{18}O concentration profiles; Arrhenius plots for F, λ, and D_{eff} using the data of Figure 3 aggregated specimen by specimen; and details of the statistical analysis procedure (PDF)

■ AUTHOR INFORMATION

Corresponding Author

Edmund G. Seebauer − *Department of Chemical and Biomolecular Engineering, University of Illinois at Urbana-Champaign, Urbana, Illinois 61801, United States;* orcid.org/0000-0002-4722-3901; Email: eseebaue@illinois.edu

Author

Heonjae Jeong − *Department of Mechanical Science and Engineering, University of Illinois at Urbana-Champaign, Urbana, Illinois 61801, United States;* orcid.org/0000-0003-4452-049X

Complete contact information is available at: https://pubs.acs.org/10.1021/acs.jpcc.2c05648

Notes

The authors declare no competing financial interest.

■ ACKNOWLEDGMENTS

This work was supported by the U.S. National Science Foundation under the grant DMR 17-09327. SIMS measurements were performed in part in the Materials Research

Laboratory Central Research Facilities, University of Illinois at Urbana-Champaign.

REFERENCES

(1) Liu, B.; Yang, J.; Wang, J.; Zhao, X.; Nakata, K. High Sub-Band Gap Response of TiO_2 Nanorod Arrays for Visible Photoelectrochemical Water Oxidation. *Appl. Surf. Sci.* **2019**, *465*, 192−200.
(2) Chinh, N. D.; Hien, T. T.; Do Van, L.; Hieu, N. M.; Quang, N. D.; Lee, S.-M.; Kim, C.; Kim, D. Adsorption/Desorption Kinetics of Nitric Oxide on Zinc Oxide Nano Film Sensor Enhanced by Light Irradiation and Gold-Nanoparticles Decoration. *Sens. Actuators, B* **2019**, *281*, 262−272.
(3) Kollmannsberger, S. L.; Walenta, C. A.; Winnerl, A.; Weiszer, S.; Pereira, R. N.; Tschurl, M.; Stutzmann, M.; Heiz, U. Doping-Dependent Adsorption and Photon-Stimulated Desorption of CO on GaN(0001). *J. Phys. Chem. C* **2017**, *121*, 8473.
(4) Khan, F.; Khan, W.; Kim, J. H.; ul Huda, N.; Salman Ajmal, H. M.; Kim, S.-D. Oxygen Desorption Kinetics of ZnO Nanorod−Gated AlGaN/GaN HEMT-Based UV Photodetectors. *AIP Adv.* **2018**, *8*, 075225.
(5) Hyodo, T.; Urata, K.; Kamada, K.; Ueda, T.; Shimizu, Y. Semiconductor-Type SnO_2-Based NO2 Sensors Operated at Room Temperature under UV-Light Irradiation. *Sens. Actuators, B* **2017**, *253*, 630−640.
(6) Hsu, C.-L.; Jhang, B.-Y.; Kao, C.; Hsueh, T.-J. UV-Illumination and Au-Nanoparticles Enhanced Gas Sensing of p-Type Na-Doped ZnO Nanowires Operating at Room Temperature. *Sens. Actuators, B* **2018**, *274*, 565−574.
(7) Tokode, O.; Prabhu, R.; Lawton, L. A.; Robertson, P. K. J. Controlled Periodic Illumination in Semiconductor Photocatalysis. *J. Photochem. Photobiol., A* **2016**, *319*−*320*, 96−106.
(8) Zhu, L.; Zeng, W. Room-Temperature Gas Sensing of ZnO-Based Gas Sensor: A Review. *Sens. Actuators, A* **2017**, *267*, 242−261.
(9) Wu, N. Plasmonic Metal−Semiconductor Photocatalysts and Photoelectrochemical Cells: A Review. *Nanoscale* **2018**, *10*, 2679−2696.
(10) Jaramillo-Quintero, O. A.; Triana, M. A.; Rincon, M. E. Optimization of Charge Transfer and Transport Processes at the CdSe Quantum Dots/TiO_2 Nanorod Interface by TiO_2 Interlayer Passivation. *J. Phys. D: Appl. Phys.* **2017**, *50*, 235305.
(11) Ammari, A.; Trari, M.; Zebbar, N. Transport Properties in Sb-Doped SnO_2 Thin Films: Effect of UV Illumination and Temperature Dependence. *Mater. Sci. Semicond. Process.* **2019**, *89*, 97−104.
(12) Saidi, T.; Palmowski, D.; Babicz-Kiewlicz, S.; Welearegay, T. G.; El Bari, N.; Ionescu, R.; Smulko, J.; Bouchikhi, B. Exhaled Breath Gas Sensing Using Pristine and Functionalized WO_3 Nanowire Sensors Enhanced by UV-Light Irradiation. *Sens. Actuators, B* **2018**, *273*, 1719−1729.
(13) Kondratenko, Y.; Seebauer, E. G. Interface-Mediated Photostimulation Effects on Diffusion and Activation of Boron Implanted into Silicon. *ECS J. Solid State Sci. Technol.* **2013**, *2*, P235−P242.
(14) Kondratenko, Y. V.; Seebauer, E. G. Directed Self-Assembly by Photostimulation of an Amorphous Semiconductor Surface. *AIChE J.* **2010**, *56*, 3206−3211.
(15) Jeong, H.; Ertekin, E.; Seebauer, E. G. Kinetic Control of Oxygen Interstitial Interaction with TiO_2(110) via the Surface Fermi Energy. *Langmuir* **2020**, *36*, 12632−12648.
(16) Jeong, H.; Li, M.; Kuang, J.; Ertekin, E.; Seebauer, E. G. Mechanism of Creation and Destruction of Oxygen Interstitial Atoms by Nonpolar Zinc Oxide(10-10) Surfaces. *Phys. Chem. Chem. Phys.* **2021**, *23*, 16423−16435.
(17) Jeong, H.; Ertekin, E.; Seebauer, E. G. Surface-Based Post-Synthesis Manipulation of Point Defects in Metal Oxides Using Liquid Water. *ACS Appl. Mater. Interfaces* **2022**, *14*, 34059−34068.
(18) Jeong, H.; Seebauer, E. G. Strong Isotopic Fractionation of Oxygen in TiO_2 Obtained by Surface-Enhanced Solid-State Diffusion. *J. Phys. Chem. Lett.* **2022**, *13*, 9841−9847.
(19) Ingebrigtsen, M. E.; Kuznetsov, A. Y.; Svensson, B. G.; Alfieri, G.; Mihaila, A.; Badstübner, U.; Perron, A.; Vines, L.; Varley, J. B. Impact of Proton Irradiation on Conductivity and Deep Level Defects in β-Ga_2O_3. *APL Mater.* **2019**, *7*, 022510.
(20) McCluskey, M. D. Point Defects in Ga_2O_3. *J. Appl. Phys.* **2020**, *127*, 101101.
(21) Kang, H. J.; Dai, P.; Campbell, B. J.; Chupas, P. J.; Rosenkranz, S.; Lee, P. L.; Huang, Q.; Li, S.; Komiya, S.; Ando, Y. Microscopic Annealing Process and Its Impact on Superconductivity in T′-Structure Electron-Doped Copper Oxides. *Nat. Mater.* **2007**, *6*, 224−229.
(22) Zhang, Y.; Cui, Z.; Zhu, L.; Zhao, Z.; Liu, H.; Wu, Q.; Wang, J.; Huang, H.; Fu, Z.; Lu, Y. Negative Effect of Oxygen Vacancies on Ferromagnetism in Ru-Doped $BaSnO_3$ Materials. *Appl. Phys. Lett.* **2020**, *117*, 052406.
(23) Zu, D.; Wang, H.; Lin, S.; Ou, G.; Wei, H.; Sun, S.; Wu, H. Oxygen-Deficient Metal Oxides: Synthesis Routes and Applications in Energy and Environment. *Nano Res.* **2019**, *12*, 2150−2163.
(24) Gorai, P.; Seebauer, E. G. Kinetic Model for Electric-Field Induced Point Defect Redistribution near Semiconductor Surfaces. *Appl. Phys. Lett.* **2014**, *105*, 021604.
(25) Gilliard, K. L.; Seebauer, E. G. Manipulation of Native Point Defect Behavior in Rutile TiO_2 via Surfaces and Extended Defects. *J. Phys.: Condens. Matter* **2017**, *29*, 445002.
(26) Narayanan, H.; Viswanathan, B.; Krishnamurthy, K. R.; Nair, H.Hydrogen from Photo-Electrocatalytic Water Splitting. *Solar Hydrogen Production*; Elsevier, 2019; pp 419−486.
(27) Gono, P.; Ambrosio, F.; Pasquarello, A. Effect of the Solvent on the Oxygen Evolution Reaction at the TiO_2−Water Interface. *J. Phys. Chem. C* **2019**, *123*, 18467−18474.
(28) Wang, D.; Sheng, T.; Chen, J.; Wang, H. F.; Hu, P. Identifying the Key Obstacle in Photocatalytic Oxygen Evolution on Rutile TiO2. *Nat. Catal.* **2018**, *1*, 291−299.
(29) Tang, J.; Durrant, J. R.; Klug, D. R. Mechanism of Photocatalytic Water Splitting in TiO_2. Reaction of Water with Photoholes, Importance of Charge Carrier Dynamics, and Evidence for Four-Hole Chemistry. *J. Am. Chem. Soc.* **2008**, *130*, 13885−13891.
(30) Ambrosio, F.; Wiktor, J.; Pasquarello, A. PH-Dependent Surface Chemistry from First Principles: Application to the BiVO4 (010)−Water Interface. *ACS Appl. Mater. Interfaces* **2018**, *10*, 10011−10021.
(31) Kafizas, A.; Godin, R.; Durrant, J. R. Charge Carrier Dynamics in Metal Oxide Photoelectrodes for Water Oxidation. *Semicond. Semimetals* **2017**, *97*, 3−46.
(32) Kanata, T.; Matsunaga, M.; Takakura, H.; Hamakawa, Y.; Nishino, T. Photoreflectance Characterization of Surface Fermi Level in As-grown GaAs(100). *J. Appl. Phys.* **1990**, *68*, 5309−5313.
(33) Shen, H.; Dutta, M. Franz−Keldysh Oscillations in Modulation Spectroscopy. *J. Appl. Phys.* **1995**, *78*, 2151−2176.
(34) Shen, H.; Zhou, W.; Pamulapati, J.; Ren, F. Photoreflectance Study of H_2S Plasma-Passivated GaAs Surface. *Appl. Phys. Lett.* **1999**, *74*, 1430−1432.
(35) Jeong, H.; Seebauer, E. G.; Ertekin, E. First-Principles Description of Oxygen Self-Diffusion in Rutile TiO_2: Assessment of Uncertainties Due to Enthalpy and Entropy Contributions. *Phys. Chem. Chem. Phys.* **2018**, *20*, 17448−17457.
(36) Seebauer, E. G.; Jung, M. Y. L.; Kwok, C. T. M.; Vaidyanathan, R.; Kondratenko, Y. V. Measurement of Photostimulated Self-Diffusion in Silicon. *J. Appl. Phys.* **2011**, *109*, 103708.
(37) Kosmulski, M. The pH Dependent Surface Charging and Points of Zero Charge. VIII. Update. *Adv. Colloid Interface Sci.* **2020**, *275*, 102064.
(38) Kosmulski, M. The pH-Dependent Surface Charging and the Points of Zero Charge. *J. Colloid Interface Sci.* **2002**, *253*, 77−87.
(39) Borghi, F.; Vyas, V.; Podestà, A.; Milani, P. Nanoscale Roughness and Morphology Affect the IsoElectric Point of Titania Surfaces. *PLoS One* **2013**, *8*, No. e68655.
(40) Dobson, K. D.; Connor, P. A.; McQuillan, A. J. Monitoring Hydrous Metal Oxide Surface Charge and Adsorption by STIRS. *Langmuir* **1997**, *13*, 2614−2616.

https://doi.org/10.1021/acs.jpcc.2c05648
J. Phys. Chem. C 2022, 126, 20800−20806

(41) Connor, P. A.; Dobson, K. D.; McQuillan, A. J. Infrared Spectroscopy of the TiO_2/Aqueous Solution Interface. *Langmuir* **1999**, *15*, 2402−2408.
(42) Bullard, J. W.; Cima, M. J. Orientation Dependence of the Isoelectric Point of TiO_2 (Rutile) Surfaces. *Langmuir* **2006**, *22*, 10264−10271.
(43) Kosmulski, M. The Significance of the Difference in the Point of Zero Charge between Rutile and Anatase. *Adv. Colloid Interface Sci.* **2002**, *99*, 255−264.

https://doi.org/10.1021/acs.jpcc.2c05648
J. Phys. Chem. C 2022, 126, 20800−20806

Supporting Information

Effects of Ultraviolet Illumination on Oxygen Interstitial Injection from TiO_2 under Liquid Water

Heonjae Jeong[1] and Edmund G. Seebauer[2]*

[1]Department of Mechanical Science and Engineering, University of Illinois at Urbana-Champaign, Urbana, Illinois 61801, United States

[2]Department of Chemical and Biomolecular Engineering, University of Illinois at Urbana-Champaign, Urbana, Illinois 61801, United States

*Corresponding author: eseebaue@illinois.edu

Supporting figures

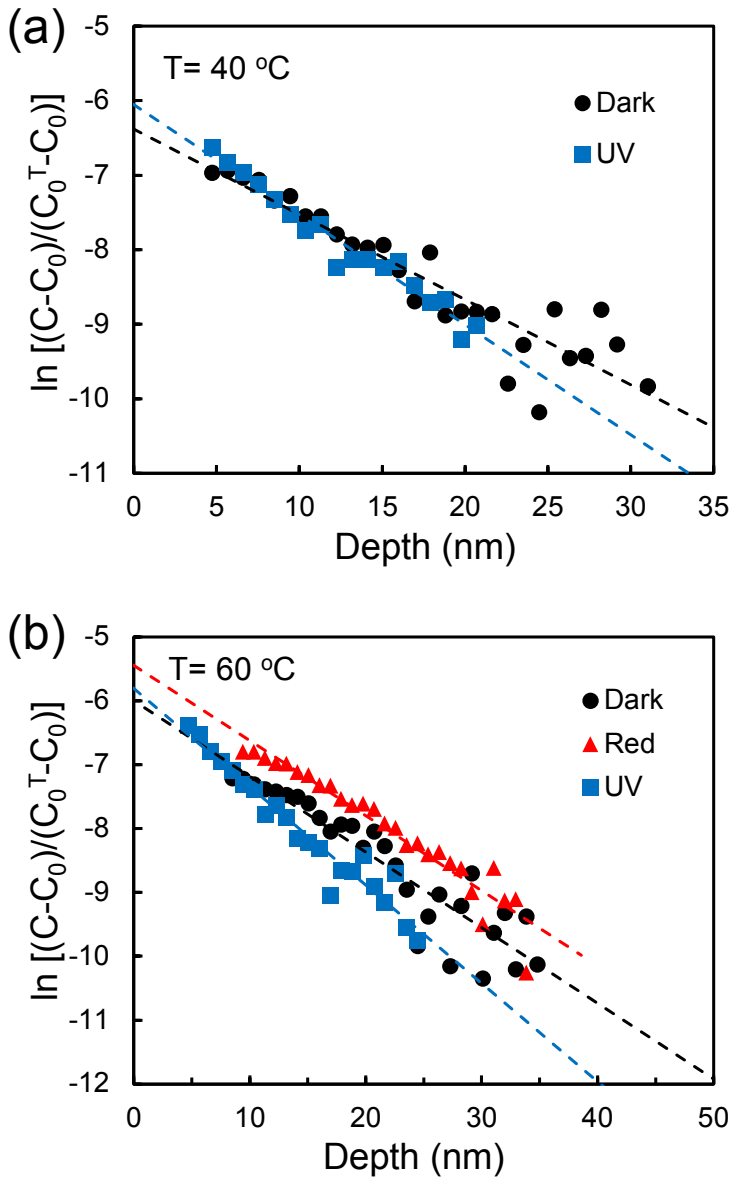

Figure S1. Representative normalized isotopic ^{18}O concentration profiles in TiO_2 at two diffusion temperatures (40 and 60 °C) under in the dark, under red (diode laser) illumination, and under UV illumination. Slopes and intercepts of the linear least-squares fits yield F and λ. Linearity of the fits is quite good.

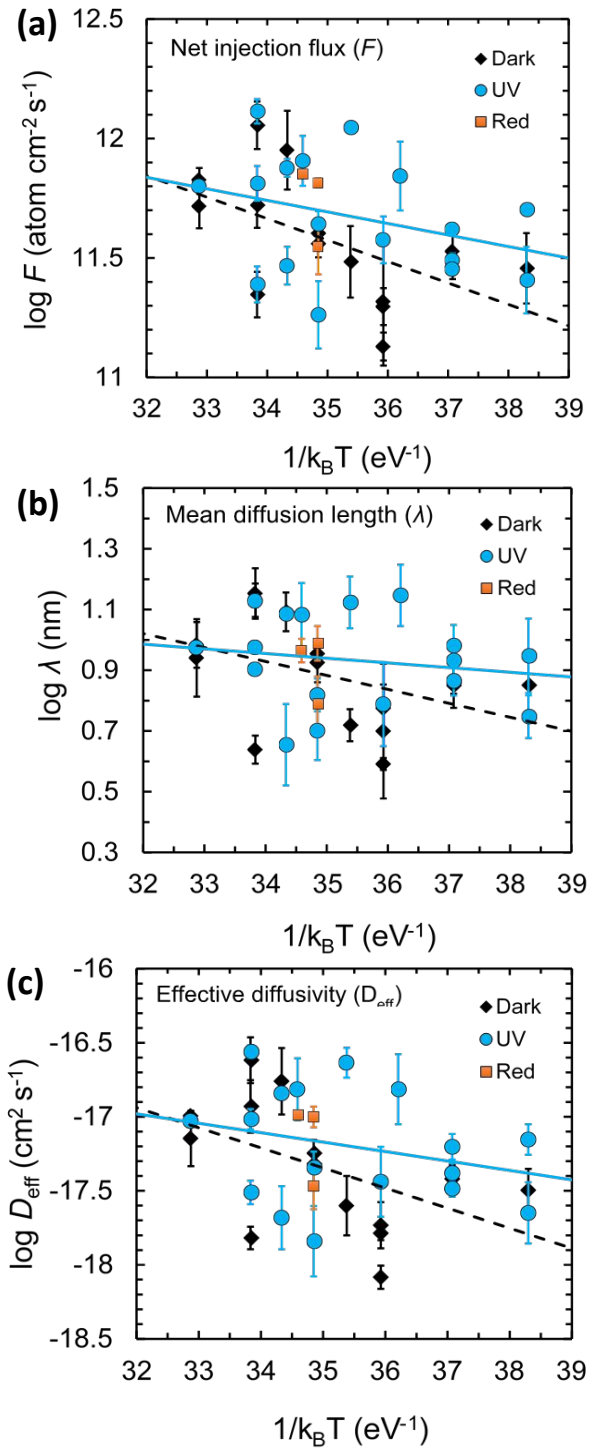

Figure S2. Arrhenius plots for (a) F, (b) λ (c) D_{eff} for TiO_2(110) using the data of Figure 3 aggregated specimen by specimen. Each point represents the average of profiles taken at two to five different locations on a single specimen's surface. Confidence intervals appear for each point; where no bars are visible, the range is narrower than the diameter of the data point. Depending upon the parameter, the confidence intervals average roughly 25 to 50% of the standard error of all points with respect to the corresponding regression line. In other words, the reproducibility on a given specimen is significantly better than between different specimens.

Details of the statistical analysis procedure

In the statistical analysis, the variances of the dark and UV data sets were assumed to be identical for each parameter, and the two sets each contained 48-49 data points. Specimens illuminated by sub-bandgap red light, which TiO_2 does not absorb appreciably, were counted as "dark" for this purpose. The results from all profiles were incorporated with equal weights.

In the comparison of mean values for each parameter, aggregating the data in different ways (for example, comparing data only at low temperature where the regression lines diverge the most) did not change the statistics appreciably because the largest differences between dark and UV conditions occur near the middle of the temperature range, as can be seen by close inspection of Figure 3.